THE JOURNAL OF PHYSICAL CHEMISTRY B

Article

pubs.acs.org/JPCB

Lifetimes of Excess Protons in Water Using a Dissociative Water Potential

Glenn K. Lockwood† and Stephen H. Garofalini*

Interfacial Molecular Science Laboratory, Department of Materials Science and Engineering, Rutgers University, 607 Taylor Rd., Piscataway, New Jersey 08855, United States

ABSTRACT: Molecular dynamics simulations using a dissociative water potential were applied to study transport of excess protons in water and determine the applicability of this potential to describe such behavior. While originally developed for gas-phase molecules and bulk liquid water, the potential is transferrable to nanoconfinement and interface scenarios. Applied here, it shows proton behavior consistent with ab initio calculations and empirical models specifically designed to describe proton transport. Both Eigen and Zundel complexes are observed in the simulations showing the Eigen−Zundel−Eigen-type mechanism. In addition to reproducing the short-time rattling of the excess proton between the two oxygens of Zundel complexes, a picosecond-scale lifetime was also found. These longer-lived H_3O^+ ions are caused by the rapid conversion of the local solvation structure around the transferring proton from a Zundel-like form to an Eigen-like form following the transfer, effectively severing the path along which the proton can rattle. The migration of H^+ over long times (>100 ps) deviates from the conventional short-time multiexponentially decaying lifetime autocorrelation model and follows the $t^{-3/2}$ power-law behavior. The potential function employed here matches many of the features of proton transport observed in ab initio molecular dynamics simulations as well as the highly developed empirical valence bond models, yet is computationally very efficient, enabling longer time and larger systems to be studied.

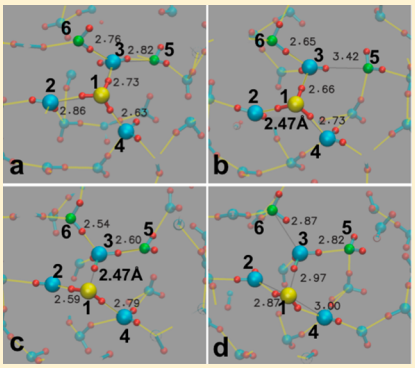

I. INTRODUCTION

Water is undoubtedly important to a wide range of sciences, and proton transport is intimately related to many of its critical functions. The behavior of protons in water and aqueous solutions governs a wealth of fundamental processes in chemistry and biology, and these processes are critical in a variety of fields such as acid-catalyzed mineral dissolution in geochemistry[1,2] or proton conductors in electrochemistry.[3−7] Shedding light on the fundamental nature of excess protons, by extension, helps us gain a better understanding of these higher-level processes.

Our understanding of proton transport in water has a long history, with experimental evidence of water's abnormally high proton conductivity being reported over a century ago.[8] Several important theories on the matter emerged to describe the solvation structures surrounding the excess proton in solution (the Eigen and Zundel configurations), and the high diffusivity of H^+ in solution has been ascribed to the Grotthuss mechanism where the excess charge migrates through proton hopping between adjacent water molecules.[9] However, these models remained uncorroborated until the relatively recent advent of accurate computer simulations and accompanying computer hardware.

Atomistic simulations using density functional theory (DFT), multistate empirical valence bond (MS-EVB) method and modifications (MS-EVB2, MS-EVB3), and other molecular dynamics (MD) simulations have confirmed that the Grotthuss mechanism is indeed the prevailing means by which excess protons move in liquid water.[10−27] A previous general conclusion was that the mechanism for these transfers involves the first-shell waters surrounding the hydronium ion in an Eigen complex breaking one of its hydrogen bonds to second shell waters, allowing formation of a Zundel complex,[9,10,12,17,28] although there are highly detailed simulations[16] and excellent experimental studies[29] that indicate that multiple hydrogen bond cleavage events participate in the structural rearrangements around the hydronium ion required for proton transport. A decrease in the barrier to transfer occurs at closer O*−O (O* is the oxygen on the hydronium ion) so that the proton can then transfer very easily, resulting in a net movement of excess charge (called "structural" diffusion) with comparatively little net molecular translation (motion of an intact hydronium ion is called "vehicular diffusion").

This Eigen-to-Zundel interconversion and proton transfer occurs readily in water.[11,30] However, only transfers followed by the severance of the hydrogen bond along which the transfer occurred result in the net migration of charge;[31,32] otherwise, a rapid back-and-forth process occurs that has been called "proton rattling".[10,12] The prevalence of this rattling behavior should give rise to a finite but transient population of Zundel states within liquid water, and indeed, recent ultrafast spectroscopic experiments have verified the presence of both Eigen and Zundel complexes in liquid water.[30]

Received: October 17, 2012
Revised: March 18, 2013
Published: April 8, 2013

The experimental methods of probing this ultrafast behavior are still emerging, and the simulation techniques traditionally used to model proton transport are sufficiently computationally expensive that system sizes on the order of 2 nm per side have often been the limit of practicality(e.g., refs 20 and 31). To this end, a dissociative molecular dynamics model of water[23] that has been shown to match a variety of bulk water properties has been applied to explore how excess protons behave in solution at statistically meaningful quantities in this work. While other recently developed dissociative water models exist,[21,22,33,34] the one we use here is also transferrable to nanoconfined water and to water reactions on oxide surfaces,[24,25,35,36] with results consistent with ab initio calculations and experiment. Those simulations[23−25] also showed proton transport, but details were never investigated. Therefore, the intent of this study was to benchmark this water model against the available knowledge from experiment and other simulations regarding proton transport and to extend this understanding into much larger systems and longer time scales to get a better understanding of the time-dependent behavior of proton transport and what factors contribute to this behavior.

II. SIMULATION TECHNIQUE

A. Interatomic Potential. Molecular dynamics simulations were carried out using a model interatomic potential composed of two- and three-body terms that allow all atoms to interact with all other atoms within a radial cutoff. As a result, no distinction between bonded and nonbonded forces is made, and protons are free to transfer between water molecules. This dissociative water potential reproduces a wide range of experimentally determined structural and dynamic properties of bulk water such as its liquid equation of state, molecular and bulk liquid structure, heat of vaporization, diffusion coefficient, and frequency spectrum[23] and is transferrable to nanoconfined water, where it uniquely reproduces the high thermal expansion of nanoconfined water seen experimentally.[35,36] It also reproduces the results of quantum mechanical simulations in different contexts including the increased hydronium ion formation near silica interfaces[24] also seen in ab initio calculations[37] and proton transport via the Grotthus mechanism along silica surfaces.[24,25]

The two-body component is composed of Coulomb interactions between point and diffuse charges ascribed to each atom, dispersion interactions, and short-range repulsion terms. Long-range Coulomb interactions are approximated by the Wolf summation method, and all interactions go to zero at interatomic spacings larger than 10 Å. To incorporate the effects of partial covalency, a Stillinger−Weber-type[38] three-body interaction is also applied to provide a relatively slight energetic bias toward the H−O−H triplet toward an angle of 104°. The form and parameters for the two- and three-body interactions can be found in our previous work.[23,25]

B. Systems. To obtain a broad sampling of hydronium behavior in water, a total of 30 liquid water systems were simulated. Twenty of these systems contained 792 H_2O molecules and one H_3O^+ ion, and the remaining 10 contained 4000 H_2O molecules and one H_3O^+ ion. These systems were created by first inserting either 792 or 4000 H_2O into a cubic simulation box sized to a density of 0.95 g/cm^3 in random locations such that no molecule−molecule pair had an oxygen−oxygen spacing less than 2.8 Å. This random mix of molecules was then simulated for 100 ps under constant temperature (298.0 K) and pressure (1 atm) by allowing the z dimension to change, and the atomic motion was propagated using the fifth-order Nordsieck−Gear method with a 0.1 fs time step. Configurations were saved every 50 fs for generating the pair distribution functions and coordination numbers in Figures 4−7 and part of Figure 9. The lifetime data and the PMFs were calculated in situ during the runs at every time step (0.1 fs) and are used in Figures 1−3 and 8 and the lifetime criteria distinguishing "short-lived" from "long-lived" in Figure 9. The coordination numbers were calculated from the minimum-to-minimum integration of the appropriate peak in the pair distribution function (PDF). For Figure 9, the PDF was generated by finding every H_3O^+ and getting the instantaneous configuration before the transfer and calculating a single PDF around that O*. After repeating this for every O* that showed the appropriate lifetime, all of those individual PDFs were averaged together, and the peak was integrated. This process was then done for all the saves immediately following the transfer.

The final configuration of each of these 30 systems was slightly different due to the density fluctuations that occur during NPT simulations, so to ensure each system of both sizes all represent the same thermodynamic macrostate, the z dimensions of these final configuration were rescaled so that all systems had the same density of 0.997 g/cm^3. For the 792-molecule system, the system dimensions were 29.219 Å × 29.219 Å × 27.872 Å, and for the 4000-molecule system, the dimensions were 50.132 Å × 50.132 Å × 47.769 Å. A single H_3O^+ molecule was then added to each of the 30 systems in a random location such that its oxygen was no closer than 2.8 Å to any neighboring oxygens, and these resulting systems were all simulated under constant temperature (T = 298.0 K) and volume for 100 ps. Although the total number of molecules in each system is increased by 1, all subsequent numerical labeling in the text and figures will refer to 792 and 4000 molecules labels. Also, in the interest of conciseness, the 792-water system will be referred to as the "small system" and the 4000-water system as the "large system".

Following this 100 ps of constant volume and constant temperature simulation, the systems were all simulated for 1.0 ns under constant volume and constant energy, and the data presented below are derived from these 1.0 ns runs. The 1 ns runs took 39 h for the 792 molecules system and 159 h for the 4000 molecules system on a single Intel Xeon X5672 processor utilizing all 4 cores.

C. Lifetimes Analysis. Calculating the lifetime of an excess proton in water is not a straightforward process because the excess proton can assume a solvation structure analogous to the Eigen complex (where the excess proton is clearly associated with one oxygen), the Zundel complex (where the excess proton is shared between two oxygens), or anything in between. Thus, attributing a specific instant at which the proton is said to have transferred is arbitrary to some degree.

To determine the lifetime of a given excess proton H^+, it is associated with its two closest oxygen ions. The closest oxygen neighbor to H^+ is defined as its donor oxygen (hereafter denoted as O*, or three-coordinated oxygen consistent with the hydronium ion), and the second-closest neighbor is defined as its acceptor oxygen. At the end of each time step, the donor and acceptor oxygens of every proton are reidentified and compared to those of the previous time step. A proton transfer is said to have occurred at that time step if (1) the proton−acceptor interatomic spacing becomes smaller than the proton−donor

dx.doi.org/10.1021/jp310300x | J. Phys. Chem. B 2013, 117, 4089−4097

spacing (i.e., $r_{OH} < r_{O^*H}$, so the identity of O* changes), *and* (2) the proton has only one oxygen (its new O*) within 1.2 Å.

The time between the transfer where an oxygen accepts an excess proton (to become an O*) and the transfer where it donates its excess proton is said to be its lifetime. O* that existed either in the initial or final configuration of the 1.0 ns simulations have lifetimes that are not exactly defined; these lifetimes are discarded.

The use of autocorrelation functions ($c_x(t)$), a method originally developed to measure hydrogen bond lifetimes,[39] is commonly used to calculate O* lifetimes.[17,18] These autocorrelation functions involve expressing the probability that a hydronium ion that exists at $t = 0$ will also be protonated at some later time t

$$c_c(t) = \frac{\langle h(0)H(t)\rangle}{\langle h\rangle} \quad (1)$$

$$c_i(t) = \frac{\langle h(0)h(t)\rangle}{\langle h\rangle} \quad (2)$$

where $H(t)$ and $h(t)$ are step functions equal to unity when the given oxygen satisfies some sort of criteria for protonation at time t and is zero otherwise. Two common forms of the autocorrelation functions are the *continuous* $c_c(t)$, where $H(t) = 1$ only if the oxygen of interest has hosted the excess proton continuously from $t = 0$ to some later time t, and the *intermittent* $c_i(t)$, where $h(t) = 1$ if the oxygen of interest is hosting an excess proton at some later time t irrespective of its protonation state between $t = 0$ and t. In the treatment presented below, we define $t = 0$ to be the time at which a proton transfer occurred and formed a new H_3O^+ ion.

Upon calculating $c_x(t)$, it can be integrated over all time to get a mean lifetime, or it can be fitted to a kinetic model from which relaxation times can be extracted. However, in choosing a form of $c_x(t)$ (intermittent or continuous) and empirical function (exponential, biexponential, and triexponential fits have all been used),[17,18] assumptions must still be made and affect the resulting lifetime measurements. So as not to make any statements as to the merit of one approach over another a priori, the results of all of these lifetime metrics are presented in this study.

Additionally, the choice of which proton-transfer events to include in these calculations is important. Ab initio molecular dynamics (AIMD) calculations have shown evidence of proton "rattling" occurring between adjacent molecules where a H_2O molecule transfers a proton to a neighboring H_2O resulting in adjacent H_3O^+ and OH^-.[40] Because the hydrogen bond (HB) along which this transfer occurs does not break, the complementary pair rapidly recombines and results in no net displacement of charge. We observe a small amount of such transient autoionization, and the recombination step ($H_3O^+ + OH^- = H_2O$) which is on the order of 100 fs can skew the short-time decay behavior of the calculated $c_x(t)$. To exclude this skew, we have chosen to examine only H^+ transfers where the acceptor oxygen is H_2O. This eliminates any autoionization reactions from the lifetime measurements since the recombination step is, by definition, a three-coordinated O* donating a proton to a hydroxyl rather than molecular water.

D. Potential of Mean Force. The free energy associated with proton transfer between H_3O^+ and an adjacent H_2O in bulk water was calculated via the potential of mean force. The final O* at $t = 1.0$ ns that originated from the initial O* from $t = 0.0$ in each of the 20 small systems was first identified, and one of its hydrogen bonds (O*–H···O, defined by $\vec{r}_{O^*H}$, $\vec{r}_{OH}$, and $\vec{r}_{O^*O}$) was arbitrarily chosen. The RATTLE algorithm with the velocity Verlet integrator[41] was then used to impose constraints on both $|r_{O^*O}|$ and $|r_{O^*H}|$ to within 0.000 01 Å. For a constrained r_{O^*O}, the associated r_{O^*H} was constrained to a specific distance and simulated for 1.0 ps under conditions of constant volume and energy. The mean restorative force (i.e., the additional force on H required to satisfy the r_{O^*H} bond constraint, or $G(r_{O^*H})$) was calculated over the final 500 fs of this constraint interval, and then r_{O^*H} was increased by 0.01 Å and the process repeated.

Each of the 20 systems underwent this procedure with five values for r_{O^*O} ranging from 2.3 to 2.7 Å, and for each r_{O^*O}, r_{O^*H} was varied from 1.00 Å to (r_{O^*O} − 1.00 Å). Because this analysis only imposed constraints on r_{O^*O} and r_{O^*H} for a single hydrogen bond of O*, there were some simulations where one of the unconstrained protons on O* incidentally transferred away during the simulation of a given r_{O^*O}. In these cases, the resulting mean force calculation then represented the autoionization energy of H_2O rather than the energy of excess proton transfer from an H_3O^+; as such, simulations exhibiting this behavior were discarded. Given the long (1.0 ps) interval per r_{O^*H}, such incidental transfers were pervasive: of the 100 PMF simulations (five values of r_{O^*O} for each of 20 systems), only 39 completed the entire range of r_{O^*H} without losing a different proton.

The potential of mean force was then calculated by taking a mean $G(r_{O^*H})$ function for each r_{O^*O} and integrating it with respect to r_{O^*H}. This integral, expressed as a function of the reaction coordinate $\delta = r_{O^*H} - r_{OH}$,[10] represents the free energy profile associated with proton transfer between O* and O molecules with the given r_{O^*O}.

III. RESULTS

A. Lifetimes. Both intermittent and continuous autocorrelation functions were calculated in both small and large systems (Figure 1). As would be expected, $c_i(t)$ decays much more slowly than $c_c(t)$, and there is negligible difference between the small and large systems in the time scales shown, indicating no finite-size effects over the time frame shown.

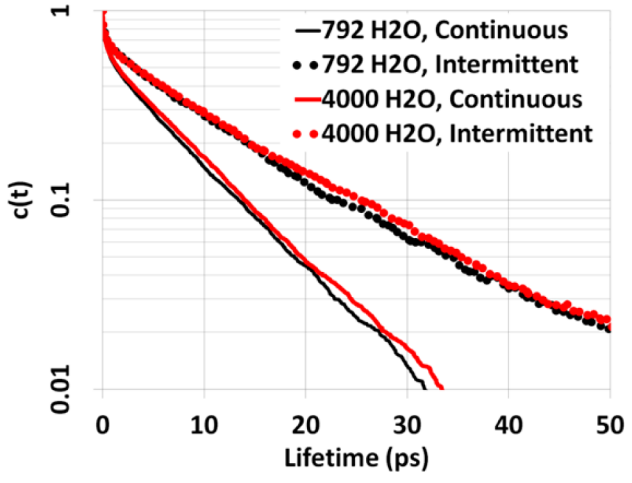

Figure 1. Continuous and intermittent $c_x(t)$ for both system sizes.

dx.doi.org/10.1021/jp310300x | J. Phys. Chem. B 2013, 117, 4089–4097

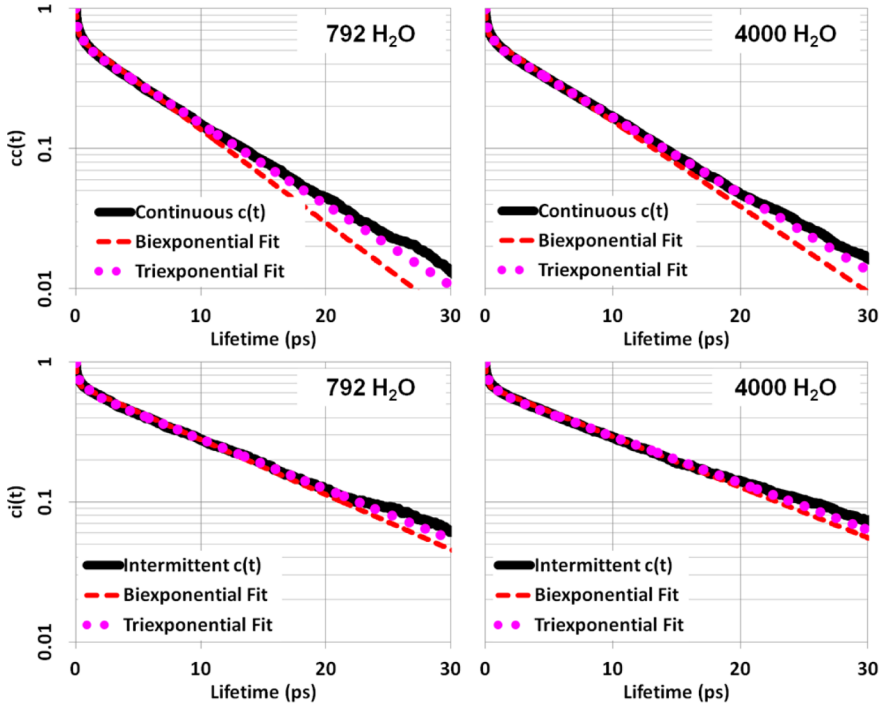

Figure 2. Calculated $c_x(t)$ and multiexponential fits.

Table 1. Multiexponential Fitting Parameters in Eq 3

$c(t)$	system size	a_1	τ_1 (ps)	a_2	τ_2 (ps)	a_3	τ_3 (ps)
continuous	792 H_2O	0.633	6.53	0.367	0.139	0	N/A
		0.568	7.53	0.214	0.0600	0.218	0.575
	4000 H_2O	0.637	7.13	0.363	0.148	0	N/A
		0.587	7.94	0.200	0.0598	0.213	0.528
intermittent	792 H_2O	0.687	11.0	0.313	0.136	0	N/A
		0.641	12.1	0.201	0.0520	0.159	0.822
	4000 H_2O	0.673	12.0	0.327	0.153	0	N/A
		0.631	13.0	0.197	0.0536	0.171	0.749

Following the biexponential model proposed by Tuckerman[31] and the triexponential model for $c_c(t)$ proposed by Markovitch et al.,[18] the following equation is fit to $c_x(t)$

$$c_x(t) = a_1 \exp\left(-\frac{1}{\tau_1}\right) + a_2 \exp\left(-\frac{t}{\tau_2}\right) + a_3 \exp\left(-\frac{t}{\tau_3}\right) \quad (3)$$

where $a_1 + a_2 + a_3 = 1.0$ and, in the biexponential case, $a_3 = 0$. The resultant fits are shown in Figure 2, with the parameters of such fits shown in Table 1 for both the continuous and intermittent $c_x(t)$. Figure 2 shows that the multiexponential correlation functions match the data in the 1−10 ps regime, similar to the findings of others.[17,20,31] Also, as shown in Figure 3 for the intermittent correlation function, the multiexponential models diverge from the calculated $c_i(t)$ after $t \sim 10-30$ ps, and the long-time behavior ($t > 10^2$ ps) follows power-law behavior (Figure 3 inset), similar to the findings of MS-EVB3 MD simulations[20] and previously shown in simulations evaluating the geminate pairs in water.[42]

In the $c_c(t)$ over 99% of O* have continuous lifetimes less than 30 ps (Figure 2). Furthermore, the triexponential fit provides a reasonable approximation of the decay behavior of $c_c(t)$ for these 99% of O* and indicates that proton transfers can be described according to three relaxation times τ of

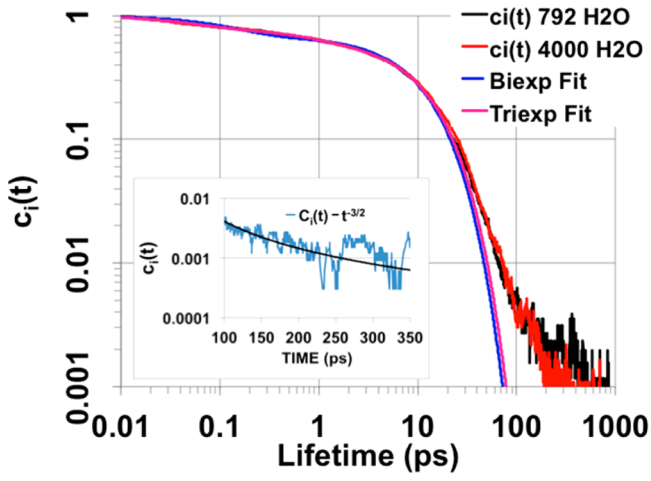

Figure 3. Intermittent $c_i(t)$ showing deviation from multiexponential fit for $t > 10^1$ ps. Inset shows that $c_i(t)$ long-time behavior (blue line) follows power-law fit of $t^{-3/2}$ (black line).

approximately 60 fs, 550 fs, and 7.7 ps. The shortest two τ values are on the same order as those reported using ab initio and MS-EVB3 simulation techniques.[20,31] However, the

dx.doi.org/10.1021/jp310300x | J. Phys. Chem. B 2013, 117, 4089−4097

relaxation time of 7.7 ps is unique to this study and represents the exponential section of $c_c(t)$ between 1 ps < t < 10 ps.

The average lifetimes over all data is 4.5 ps in the small systems and 4.8 ps in the large systems. This is a factor of 2.5 larger than the experimental value.[9,43] Hofer et al. calculated the diffusion coefficient of the excess proton using this dissociative water potential,[27] finding a value of 0.39 Å^2/ps. In their paper, they compared this diffusion constant to the experimental value (0.93 Å^2/ps) and to the various versions of MS-EVB, with MS-EVB (0.35 Å^2/ps,[15] 0.77 Å^2/ps,[14] 0.83 Å^2/ps[44]), MS-EVB2 (0.36 Å^2/ps[19]), and MS-EVB3 (0.29 Å^2/ps[19]).

B. Local Structure. Given the set of O* and their lifetimes calculated in section IIIA above, the O*−O and O*−H pair distribution functions (PDFs) were calculated around each O* over its lifetime. Because the O* included in section IIIA only considers O* that deprotonated by transferring the excess proton to H_2O (as opposed to OH^-), the following PDF data exclude transient H_3O^+ that formed from proton rattling between adjacent H_2O molecules. Additionally, PDF sampling was performed every 50 fs, so any extremely short-lived O* that formed and deprotonated between sampling intervals are not included. Finally, although these analyses were performed on both small and large system sets, only results from the small systems are presented as the large-system data was negligibly different.

1. Average Structure. Figure 4 shows the overall local structure surrounding O* in comparison to the average

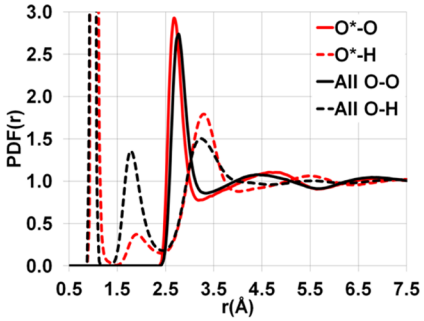

Figure 4. Radial distribution functions for oxygen coordinated as H_3O^+ (O*) and oxygen coordinated in any form from 792-water systems. All systems were sampled every 50 fs.

structure surrounding all O, the vast majority of which is H_2O. As indicated in previous work,[23] the dissociative water potential used here produces PDFs for liquid water that are in excellent agreement with experiment.[45] The O*−O PDF shows a shift to shorter distances for the first peak and an increase in the distance for the second peak in comparison to the O−O data from all oxygen (labeled All O−O). This is also consistent with the slightly elongated O*−H first peak in comparison to the data from all O−H (labeled "All O−H"). The greater amplitude of the O*−H distance would be able to attract a neighboring O, causing the decreased O*−O spacing. This shortened O*−O spacing is consistent with the results from the MS-EVB3 potential.[18]

The second-neighbor O*−H HB acceptor peak around r = 1.8 Å is significantly lower around O* due to the fact that H_3O^+ can only accept one HB whereas H_2O can accept two. Integrating the PDF over this second peak indicates that the H_3O^+ accepts an average 0.66 HB whereas the systemwide HB acceptor average is 1.89 per molecule overall.

The magnitude of this O*−O shift is significantly less than the 0.2 Å inward shift predicted by the empirical potential structure refinement (EPSR) of neutron scattering data.[46] However, the EPSR method prescribes a rigid molecular geometry for both H_2O and H_3O^+ a priori, and this limitation prevents the EPSR-derived PDFs from reflecting the intermediate-range effects of O−H bonds responding to changing solvation patterns. As a consequence, the Zundel structure, experimentally observed via other means,[30,47] is not represented in these EPSR-derived PDFs, and the loss of these O−H dynamics may cause the exaggerated inward shift of this O−O peak shown in EPSR.

2. Lifetime-Dependent Structure. Because the $c_c(t)$ fitting described in section IIIA above suggests the existence of several time scales over which O* deprotonates, the O*−X PDFs over species that only show short- or long-lived behavior may elucidate the structural properties that govern these different lifetimes.

The results of such an analysis for the O*−H pair is shown in Figure 5, which shows that protons surrounding short-lived

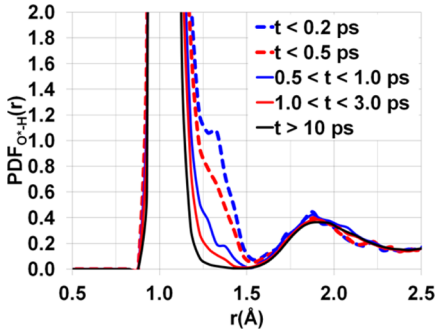

Figure 5. First and second peaks in the O*−H PDF calculated over O* that showed different lifetimes t.

O* sample a much greater volume between neighboring oxygens than long-lived O*. The shortest-lived O* (t < 0.2 ps) demonstrate a split first O*−H peak, indicative of the Zundel cation structure predicted by AIMD[12] and later observed with MS-EVB3,[18] again showing that our results are consistent with AIMD and the MS-EVB3 model, both of which are much more computationally intensive than our simulations. However, the disappearance of this second peak around longer-lived O* indicates that the excess proton does not spend the majority of its time in a Zundel complex. Rather, the Eigen form shows greater stability and contribution to the overall O*−H PDF during the lifetime of O*, and the Zundel exists as an intermediate form that occurs during the proton-transfer process. These observations are consistent with both computational and experimental findings.[9,18,48]

The O*−O PDFs shown in Figure 6 show that the short-lived O* exhibit a shift in this first solvation shell toward shorter O*−O spacings relative to longer-lived O*. Additionally, they occupy very short (r_{O^*O} < 2.44 Å) distances with greater frequency (inset of Figure 6) which is again indicative of Zundel-like structure. By comparison, the long-lived (t > 10 ps) O* show overall greater structure in this first solvation shell.

The shortest-lived O* have appreciably shorter O*−O spacing at intermediate distances as well (Figure 7) and it follows that the overall atomic density surrounding these short-lived ions is higher. This higher-density environment extends at least 5.5 Å from O* which indicates that the transfer process

dx.doi.org/10.1021/jp310300x | J. Phys. Chem. B 2013, 117, 4089−4097

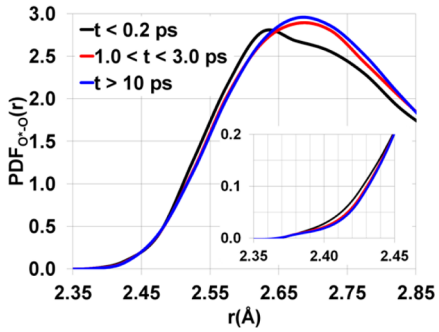

Figure 6. First peak of the O*−O PDF. Inset shows the lower limit of O*−O spacing observed.

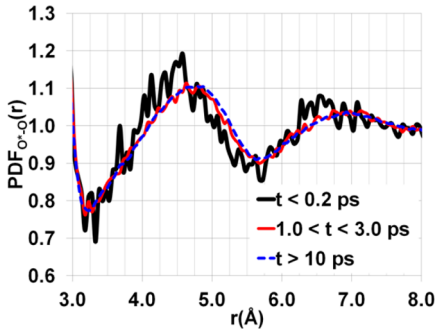

Figure 7. Second and third peaks in O*−O PDF over O* that showed different lifetimes *t*.

alters both the first and second solvation shells. This is in very good agreement with simulations and experiments that have shown that the excess proton affects the structure of multiple solvation shells.[16,29]

Unlike the first O*−O peak, the difference in local density between intermediate- and long-lived O* is far less pronounced. The second and third O*−O PDF peaks for lifetimes between 1 and 3 ps are only marginally closer than those ions lasting more than 10 ps, suggesting that all ions with lifetimes >1.0 ps deprotonate according to a common mechanism. This is consistent with the findings of section IIIA above where $c_c(t)$ exhibits only one decay behavior with a characteristic relaxation time $\tau > 1$ ps.

C. Barrier to Transfer. The free energy barrier for proton transfer in bulk water was calculated using the potential of mean force for various r_{O^*O} (Figure 8). For $r_{O^*O} = 2.7$ Å, which corresponds to the first-neighbor maximum in the O*−O PDF (Figure 6), the barrier for deprotonation approaches 1.6 kcal/mol (3kT) at O−H distances corresponding to 1.23 Å. The

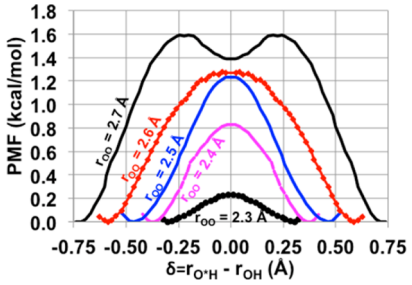

Figure 8. Potential of mean force for proton transfer between H_3O^+ and H_2O, symmetrized around $\delta = 0$, where $\delta = r_{O^*H} - r_{OH}$ is the reaction coordinate.

metastable region around $\delta = 0.0$ that is present at this distance (as well as smaller r_{O^*O} in the vapor phase Zundel, not shown) is an artifact of the two constraints; two H_2O sharing an excess proton at $r_{O^*O} = 2.7$ Å would quickly contract to shorter O*−O spacings and cause this metastable point to disappear.

The barrier begins to decrease for $r_{O^*O} < 2.5$ Å and shows evidence of going to zero for very small r_{O^*O} which is consistent with ab initio calculations.[49] In the simulations conducted here, the minimum typical r_{O^*O} immediately preceding proton transfer is 2.4 Å, which corresponds to an activation barrier of 0.8 kcal/mol. This barrier is in generally good agreement with AIMD calculations using classical protons which give a value of 0.6 kcal/mol.[12] Marx et al.,[12] as well as Tuckerman et al.,[28] state that the zero-point motion of the proton would lower the barrier.

IV. DISCUSSION

The simulations show that this dissociative water potential that was designed for bulk water has properties that enable descriptions of proton transfer that are consistent with a number of results from either ab initio calculations or potentials specifically designed for proton transfer (MS-EVB versions).

The simulations presented here reveal two general time domains for proton transfer: one on the order of tens to hundreds of femtoseconds and the other on the order of picoseconds. The femtosecond-scale lifetimes, also seen in AIMD and MS-EVB MD, are the result of rapid back-and-forth rattling of protons and can be decomposed into subdomains on the order of 10^1 and 10^2 fs. The local structure around these femtosecond-scale O* indicates that these sites maintain a Zundel-like environment marked by a bimodal O*−H first neighbor distance caused by the transferring proton. These short-lived O* also feature a shorter O*−O first-neighbor distance as evidenced by the O*O PDF (Figure 6), and these shorter O*−O distances reduce the barrier for transfer and allow the observed rattling to take place.

A significant number of O* remained continuously protonated with lifetimes on the order of picoseconds, as observed in experiment.[43] These longer-lived O* exhibit structure more consistent with an Eigen-like complex with three strongly hydrogen-bonded acceptor neighbors, confirming that the Eigen cation is the more stable solvation structure around the excess proton in solution.

Until this point in the discussion, it remains unclear what causes some O* to have very long lifetimes; all that can be said is that those O* with very *short* lifetimes are cases of proton rattling. However, the second peak in the O*−H PDF (Figure 5) is invariant with respect to the lifetime of the central O* and indicates that both Eigen and Zundel complexes accept fewer than one HB on average. While this observation is intuitive in the case of the Eigen cation which donates three HBs, it also indicates that both oxygen ions in the Zundel complex accept less than one HB; if this was not the case, the PDF of short-lived O* would show a higher second-neighbor O*H peak due to the identity of O* switching during rattling.

This notion that rattling occurs when both donor and acceptor oxygens are HB deficient follows the AIMD-derived model of presolvation,[50] where transfer only occurs when the environment around the acceptor O is similar to O*. To confirm this, the coordination of each acceptor O can be calculated immediately before the formation of what will be a short-lived O* (lifetime <200 fs) and compared to the average coordination around O* and O (Figure 9). Indeed,

dx.doi.org/10.1021/jp310300x | J. Phys. Chem. B 2013, 117, 4089−4097

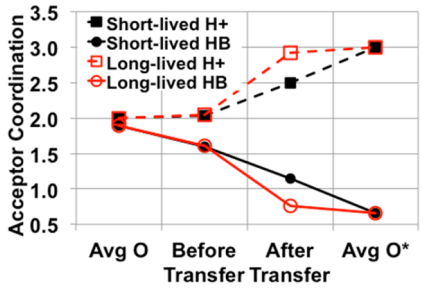

Figure 9. Average proton and hydrogen bond coordination around O and O* immediately before and immediately after proton transfer. Structural sampling was conducted every 50 fs, so "immediately" means within 50 fs, and for a given transfer event, the sum of the time before and time after transfer equals this 50 fs.

immediately (less than 50 fs) before a short-lived O* accepts its excess proton, this accepting H_2O oxygen already shows reduced HB coordination, and the average HB coordination continues to decrease immediately after the transfer event.

The formation of long-lived O* (lifetime >10 ps) shows similar indicators of presolvation where the average HB coordination immediately preceding the transfer is reduced. However, the coordination of long-lived O* changes much more rapidly immediately after the transfer, and it already resembles the overall Eigen-like average HB coordination within 50 fs posttransfer. Thus, the long-lived O* are long-lived by virtue of the fact that the HB along which the proton transfer took place is rapidly severed within 50 fs of the transfer, preventing the reverse transfer and the observation of proton rattling. Only 9.1% of these long-lived O* transferred back to their original donors; by comparison, 75% of short-lived O* transferred back. "Presolvation" may be a term describing a moment in the dynamic nature of proton transfer. Using MS-EVB models, others have attributed this transfer process to a "special pair dance", in which various first-shell waters are approached prior to one of them becoming the proton acceptor.[16,18] Figure 10 shows several snapshots from a movie in our simulations that shows proton transfer after the H_3O^+ ion sampled more than one first shell waters (water 2 in (b), then water 3 in (c)). Water 2 is apparently not in the correct orientation to accept the proton in (b), but the structure in (b) looks like a distorted Eigen complex discussed by Markovitch et al.[18] In the particular scenario shown in Figure 10, transfer to 3 was initiated by the motion of water 5 (a second shell water), first away from 3 in Figure 10b, then returning to 3 and whose momentum caused 3 to move sufficiently close to O* at the correct orientation to accept the excess proton (Figure 10c). In Figure 10c, 3 is not in a "presolvation" configuration because of the H-bond with 6. However, Figure 10d shows that the 3−6 H-bond is broken almost immediately.

V. CONCLUSIONS

A dissociative water potential that reproduces multiple bulk water properties and is transferrable to nanoconfined water and

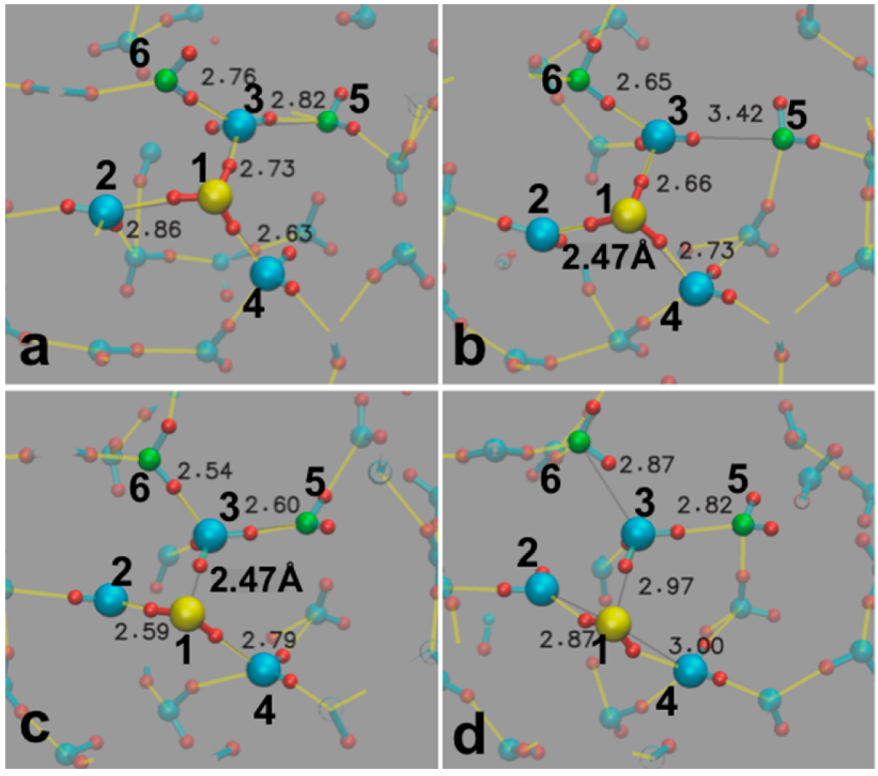

Figure 10. Snapshots of the evolution of proton transfer from the H_3O^+ ion (yellow O* labeled 1) showing the dynamic nature of transfer and the sampling of multiple first-shell waters (large blue) prior to transfer. Smallest numbers indicate O−O spacing between specific pairs. (a) O* hydrogen-bonded to waters 2, 3, 4 in an Eigen complex, (b) O*−2 distance decreases to 2.47 Å, but no transfer occurs and 3−5 distance increases (broken first- and second-shell hydrogen bond), (c) 5 moves back toward 3, eventually pushing it toward O*, where the transfer occurs between O* and 3 as the distance decreases to 2.47 Å and 3 becomes the new O*, (d) the 3−6 H-bond breaks. Third-shell waters (green) play a role in the movement of 5 away from 3, then back toward 3. Yellow lines are H-bonds, and thin black lines indicate pairs over which distances are calculated in VMD.

dx.doi.org/10.1021/jp310300x | J. Phys. Chem. B 2013, 117, 4089−4097

water reactions on silica surfaces has been applied in molecular dynamics simulations to determine its applicability for studying the transfer of an excess proton in solution. While the potential was not originally designed for proton transfer, results shown here are nonetheless consistent with proton behavior observed in ab initio calculations or in simulations using potentials specifically designed to reproduce proton transfer (MS-EVB models). An important feature in the current simulations is that this model is computationally much faster than ab initio and MS-EVB models. Fitting exponential models to the resulting proton autocorrelation functions reveals that the lifetimes of O* are best represented by several time scales: two in the femtosecond scale and one in the picosecond scale.

The femtosecond scale lifetimes are consistent with the lifetimes observed in both quantum-mechanical and empirical valence bond calculations. These short lifetimes are the result of protons rattling between the two oxygens of Zundel complexes and are marked by an inward shift of the O*O PDF that is clearly evident in both first and second solvation shells. The PMF calculations show that this closer O*O spacing results in a reduced barrier to transfer, similar to the ab initio calculations, and permits the proton to rapidly transfer back and forth with no net transport of charge. This decrease in the barrier to proton transfer with decreasing O*O spacing during the transformation of the Eigen complex to the Zundel complex enables the transfers seen in these simulations, regardless of lifetime.

The picosecond-scale O* lifetimes are the result of the severing of the hydrogen bond along which the transfer occurred within 50 fs of the transfer and are marked by an outward shift in spacing of atomic density and a higher barrier to transfer. Transfers via these long-lived O* are what contribute to net migration of charge, and the long-time behavior of this motion (expressed in the intermittent autocorrelation function) matches the predictions of the MS-EVB models including the nonexponential decay at times greater than 100 ps with the −3/2 power-law behavior consistent with diffusive behavior.

AUTHOR INFORMATION

Corresponding Author

*Tel.: 848 445-2216. E-mail: shg@rutgers.edu.

Present Address

[†]San Diego Supercomputer Center, UC San Diego, La Jolla, CA 92093.

Notes

The authors declare no competing financial interest.

REFERENCES

(1) Adeagbo, W. A.; Doltsinis, N. L.; Klevakina, K.; Renner, J. Transport Processes at Alpha-Quartz-Water Interfaces: Insights from First-Principles Molecular Dynamics Simulations. *ChemPhysChem* **2008**, *9*, 994−1002.

(2) Criscenti, L. J.; Kubicki, J. D.; Brantley, S. L. Silicate Glass and Mineral Dissolution: Calculated Reaction Paths and Activation Energies for Hydrolysis of a Q_3 Si by H_3O^+ Using Ab Initio Methods. *J. Phys. Chem. A* **2006**, *110*, 198−206.

(3) Nogami, M.; Abe, Y. Evidence of Water-Cooperative Proton Conduction in Silica Glass. *Phys. Rev. B* **1997**, *55*, 12108−12112.

(4) Nogami, M.; Nagao, R.; Wong, C. Proton Conduction in Porous Silica Glasses with High Water Content. *J. Phys. Chem.* **1998**, *102*, 5772−5775.

(5) Nogami, M. Proton Conduction in Nanopore-Controlled Silica Glasses. *J. Sol-Gel Sci. Technol.* **2004**, *31*, 359−364.

(6) Nogami, M.; Matsushita, H.; Goto, Y.; Kasuga, T. A Sol-Gel-Derived Glass as a Fuel Cell Electrolyte. *Adv. Mater.* **2000**, *12*, 1370−1372.

(7) Colomer, M. T.; Rubio, F.; Jurado, J. R. Transport Properties of Fast Proton Conducting Mesoporous Silica Xerogels. *J. Power Sources* **2007**, *167*, 53−57.

(8) Johnston, J. The Change of the Equivalent Conductance of Ions with the Temperature. *J. Am. Chem. Soc.* **1909**, *31*, 1010−1020.

(9) Agmon, N. The Grotthuss Mechanism. *Chem. Phys. Lett.* **1995**, *244*, 456−462.

(10) Marx, D.; Tuckerman, M. E.; Hutter, J.; Parrinello, M. The Nature of the Hydrated Excess Proton in Water. *Nature* **1999**, *397*, 601−604.

(11) Tuckerman, M.; Laasonen, K.; Sprik, M.; Parrinello, M. Ab-Initio Molecular Dynamics Simulation of the Solvation and Transport of H_3O^+ and OH^- Ions in Water. *J. Phys. Chem.* **1995**, *99*, 5749−5752.

(12) Marx, D.; Tuckerman, M. E.; Parrinello, M. Solvated Excess Protons in Water: Quantum Effects on the Hydration Structure. *J. Phys.: Condens. Matter* **2000**, *12*, A153−A159.

(13) Vuilleumier, R.; Borgis, D. Quantum Dynamics of an Excess Proton in Water Using an Extended Empirical Valence-Bond Hamiltonian. *J. Phys. Chem. B* **1998**, *102*, 4261−4264.

(14) Vuilleumier, R.; Borgis, D. Transport and Spectroscopy of the Hydrated Proton: A Molecular Dynamics Study. *J. Chem . Phys.* **1999**, *111*, 4251−4266.

(15) Cuma, M.; Schmitt, U. W.; Voth, G. A. A Multi-State Empirical Valence Bond Model for Weak Acid Dissociation in Aqueous Solution. *J. Phys. Chem. A* **2001**, *105*, 2814−2823.

(16) Lapid, H.; Agmon, N.; Petersen, M. K.; Voth, G. A. A Bond-Order Analysis of the Mechanism for Hydrated Proton Mobility in Liquid Water. *J. Chem. Phys.* **2005**, *122*, 14506.

(17) Chandra, A.; Tuckerman, M. E.; Marx, D. Connecting Solvation Shell Structure to Proton Transport Kinetics in Hydrogen-Bonded Networks Via Population Correlation Functions. *Phys. Rev. Lett.* **2007**, *99*, 145901.

(18) Markovitch, O.; Chen, H.; Izvekov, S.; Paesani, F.; Voth, G. A.; Agmon, N. Special Pair Dance and Partner Selection: Elementary Steps in Proton Transport in Liquid Water. *J. Phys. Chem. B* **2008**, *112*, 9456−9466.

(19) Wu, Y.; Chen, H.; Wang, F.; Paesani, F.; Voth, G. A. An Improved Multistate Empirical Valence Bond Model for Aqueous Proton Solvation and Transport. *J. Phys. Chem. B* **2008**, *112*, 467−482.

(20) Chen, H.; Voth, G. A.; Agmon, N. Kinetics of Proton Migration in Liquid Water. *J. Phys. Chem. B* **2010**, *114*, 333−339.

(21) Park, K.; Lin, W.; Paesani, F. A Refined MS-EVB Model for Proton Transport in Aqueous Environments. *J. Phys. Chem. B* **2012**, *116*, 343−352.

(22) Lee, S. H.; Rasaiah, J. C. Proton Transfer and the Mobilities of the $H^+$and OH^-Ions from Studies of a Dissociating Model for Water. *J. Chem . Phys.* **2011**, *135*, 124505.

(23) Mahadevan, T. S.; Garofalini, S. H. Dissociative Water Potential for Molecular Dynamics Simulations. *J. Phys. Chem. B* **2007**, *111*, 8919−8927.

(24) Mahadevan, T. S.; Garofalini, S. H. Dissociative Chemisorption of Water onto Silica Surfaces and Formation of Hydronium Ions. *J. Phys. Chem. C* **2008**, *112*, 1507−1515.

(25) Lockwood, G. K.; Garofalini, S. H. Bridging Oxygen as a Site for Proton Adsorption on the Vitreous Silica Surface. *J. Chem. Phys.* **2009**, *131*, 074703.

(26) Lockwood, G. K.; Garofalini, S. H. Effect of Moisture on the Self-Healing of Vitreous Silica under Irradiation. *J. Nucl. Mater.* **2010**, *400*, 73−78.

(27) Hofer, T.; Hitzenberger, M.; Randolf, B. Combining a Dissociative Water Model with a Hybrid QM/MM Approach-a Simulation Strategy for the Study of Proton Transfer Reactions in Solution. *J. Chem. Theory Comput.* **2012**, *8*, 3586−3595.

(28) Tuckerman, M. E.; Marx, D.; Klein, M. L.; Parrinello, M. On the Quantum Nature of the Shared Proton in Hydrogen Bonds. *Science* **1997**, *275*, 817−820.

(29) Tielrooij, K. J.; Timmer, R. L. A.; Bakker, H. J.; Bonn, M. Structure Dynamics of the Proton in Liquid Water Probed with Terahertz Time-Domain Spectroscopy. *Phys. Rev. Lett.* **2009**, *102*, 198303.
(30) Woutersen, S.; Bakker, H. J. Ultrafast Vibrational and Structural Dynamics of the Protons in Liquid Water. *Phys. Rev. Lett.* **2006**, *96*, 138305.
(31) Tuckerman, M. E.; Chandra, A.; Marx, D. A Statistical Mechanical Theory of Proton Transport Kinetics in Hydrogen-Bonded Networks Based on Population Correlation Functions with Applications to Acids and Bases. *J. Chem. Phys.* **2010**, *133*, 124108.
(32) Marx, D.; Chandra, A.; Tuckerman, M. E. Aqueous Basic Solutions: Hydroxide Solvation, Structural Diffusion, and Comparison to the Hydrated Proton. *Chem. Rev.* **2010**, *110*, 2174−2216.
(33) Kale, S.; Herzfeld, J.; Dai, S.; Blank, M. Lewis-Inspired Representation of Dissociable Water in Clusters and Grotthus Chains. *J. Biol. Phys.* **2012**, *38*, 49−59.
(34) Lussetti, E.; Pastore, G.; Smargiassi, E. A Fully Polarizable and Dissociable Potential for Water. *Chem. Phys. Lett.* **2003**, *381*, 287−291.
(35) Garofalini, S. H.; Mahadevan, T. S.; Xu, S.; Scherer, G. W. Molecular Mechanisms Causing Anomalously High Thermal Expansion of Nanoconfined Water. *ChemPhysChem* **2008**, *9*, 1997−2001.
(36) Xu, S.; Scherer, G. W.; Mahadevan, T. S.; Garofalini, S. H. Thermal Expansion of Confined Water. *Langmuir* **2009**, *25*, 5076−5083.
(37) Ma, Y.; Foster, A. S.; Nieminen, R. M. Reactions and Clustering of Water with Silica Surface. *J. Chem. Phys.* **2005**, *122*, 144709.
(38) Stillinger, F. H.; Weber, T. A. Computer Simulation of Local Order in Condensed Phases of Silicon. *Phys. Rev. B* **1985**, *31*, 5262−5271.
(39) Rapaport, D. C. Hydrogen Bonds in Water. *Mol. Phys.* **1983**, *50*, 1151−1162.
(40) Geissler, P. L.; Dellago, C.; Chandler, D.; Hutter, J.; Parrinello, M. Autoionization in Liquid Water. *Science* **2001**, *291*, 2121−2124.
(41) Andersen, H. C. Rattle: A "Velocity" Version of the Shake Algorithm for Molecular Dynamics Calculations. *J. Comput. Phys.* **1983**, *52*, 24−34.
(42) Markovitch, O.; Agmon, N. Reversible Geminate Recombination of Hydrogen-Bonded Water Molecule Pair. *J. Chem . Phys.* **2008**, *129*, 084505−084505.
(43) Luz, Z.; Meiboom, S. The Activation Energies of Proton Transfer Reactions in Water. *J. Am. Chem. Soc.* **1964**, *86*, 4768−4769.
(44) Brancato, G.; Tuckerman, M. E. A Polarizable Multistate Empirical Valence Bond Model for Proton Transport in Aqueous Solution. *J. Chem . Phys.* **2005**, *122*, 224507.
(45) Soper, A. K.; Ricci, M. A. Structures of High-Density and Low-Density Water. *Phys. Rev. Lett.* **2000**, *84*, 2881−2884.
(46) Botti, A.; Bruni, F.; Imberti, S.; Ricci, M. A.; Soper, A. K. Ions in Water: The Microscopic Structure of Concentrated Hcl Solution. *J. Chem. Phys.* **2004**, *121*, 7840−7848.
(47) Headrick, J. M.; Diken, E. G.; Walters, R. S.; Hammer, N. I.; Christie, R. A.; Cui, J.; Myshakin, E. M.; Duncan, M. A.; Johnson, M. A.; Jordan, K. D. Spectral Signatures of Hydrated Proton Vibrations in Water Clusters. *Science* **2005**, *308*, 1765−1769.
(48) Winter, B.; Faubel, M.; Hertel, I. V.; Pettenkofer, C.; Bradford, S. E.; Jagoda-Cwiklik, B.; Cwiklik, L.; Jungwirth, P. Electron Binding Energies of Hydrated $H_3O^+$and OH^-: Photoelectron Spectroscopy of Aqueous Acid and Base Solutions Combined with Electronic Structure Calculations. *J. Am. Chem. Soc.* **2006**, *128*, 3864−3865.
(49) Marx, D. Proton Transfer 200 Years after Von Grotthuss: Insights from Ab Initio Simulations. *ChemPhysChem* **2006**, *7*, 1848−1870.
(50) Tuckerman, M. E.; Marx, D.; Parrinello, M. The Nature and Transport Mechanism of Hydrated Hydroxide Ions in Aqueous Solution. *Nature* **2002**, *417*, 925−929.